Theoretical studies of sonoluminescence radiation: Radiative transfer and parametric dependence

L. Kondić,* Joel I. Gersten, and Chi Yuan†
City College of The City University of New York, New York, New York 10031
(Received 21 December 1994; revised manuscript received 11 May 1995)

We present results for sonoluminescent (SL) radiation from a strongly modulated air bubble in water. The SL pulse is due to high temperatures in the bubble produced by the collapse of a shock wave. The dependence of SL radiation on acoustic pressure and initial bubble size is discussed, as well as the inclusion of various mechanical energy loss mechanisms. We find that inclusion of loss terms, especially due to radiation, is necessary in order to understand the bubble dynamics, the resulting SL pulse, and some recent experiments.

PACS number(s): 47.55.Bx, 78.60.Mq, 44.40.+a, 47.40.−x

INTRODUCTION

Sonoluminescence (SL) has been the object of considerable study for more than 60 years [1]. Recently [2] it was found that the brief flashes of light that are produced are of very short duration (less than 50 ps) and have a broad spectral range associated with them, spanning at least the visible spectrum and extending into the ultraviolet. The duration of the flashes was found to be sufficiently short to rule out conventional radiative relaxation processes (requiring times of the order of 1 ns or more). The energy spectrum was sufficiently broad to eliminate superradiance, superfluorescence, or laser-type mechanisms, which rely on a high number of photons occupying a single optical mode. More recently [3] the spectrum of the flashes was found to be consistent with a blackbody spectrum. Furthermore [4], detailed measurements of the radius of the bubble as a function of time have shown that the wall of the bubble might achieve supersonic speeds prior to the onset of luminescence. It has been proposed that SL is associated with the production of shock waves in the gas inside the bubble [4]. Theoretical calculations, based on the gas dynamic equations coupled to the bubble wall dynamics, have found shock waves [5–7] as well. The predicted high temperatures, coupled with a bremsstrahlung mechanism, were used to explain SL. We find that the inclusion of various physical processes such as dissociation, ionization, and radiation in the problem have considerable importance and that it is necessary in order to fully understand the physics of collapsing sonoluminescent bubbles. We also compare our results with recent experimental data [8]. This paper is organized as follows. In Sec. I we formulate the model. The subject of Sec. II will be the inclusion of the loss terms mentioned above. Section III gives a comparison of the results with and without corrections as well as a discussion of the changes in the results for different experimental parameters. Finally, in Sec. IV we present results for sonoluminescent radiation. We would like to point out that due to the complexity of the problem, especially the self-consistent radiation-matter coupling (the subject of Sec. II), we make some simplifications here in order to keep the model solvable.

I. FORMULATION OF THE PROBLEM

The physical problem is an air bubble in water, of equilibrium size of about $4\,\mu$m, subjected to a periodic spherical sound wave of ultrasound frequency (typically 20 kHz) and an acoustic amplitude of about $1.2 - 1.3$ atm. The motion of the bubble wall follows from the equation [9]

$$R\ddot{R} + \frac{3}{2}\dot{R}^2 = \frac{1}{\rho_l}[P_g(t) - P_a(t) - P_0] + \frac{R}{\rho_l c_l}\frac{d}{dt}[P_g(R) - P_a(t)] - 4\nu_l\frac{\dot{R}}{R}. \quad (1)$$

This equation, without the acoustic damping term, is known as Rayleigh-Plesset (RP) equation. Here $P_g(t)$ is the pressure in the gas next to the bubble wall, $P_a(t)$ is the acoustic pressure given by $P_a(t) = P_a \sin(\omega_a t)$, P_0 is the hydrostatic pressure, ρ_l is the density of the liquid, c_l is the speed of sound in the liquid, and ν_l is its kinematic viscosity. Additional terms resulting from the compressibility of the liquid have been neglected, as well as the possibility of heat conduction and mass diffusion. It is worth noting that during most of the collapse of the bubble, when all terms on the right-hand side of Eq. (1) are very small (compared with the terms on the left-hand side), the motion of the bubble wall basically follows Rayleigh's solution [10] for the collapse of an empty cavity. This is given by $R(t) \sim (1 - t/t_0)^{2/5}$, where t_0 is the collapse time if the gas in the bubble did nothing to influence the motion of the bubble wall. For Fig. 1, this

*Present address: Courant Institute of Mathematical Sciences, New York University, New York, NY 10012; e-mail: KONDICECIMS.NYU.EDU
†Present address: Institute of Astronomy and Astrophysics, Academia Sinica, Nankang, Taiwan, Republic of China.

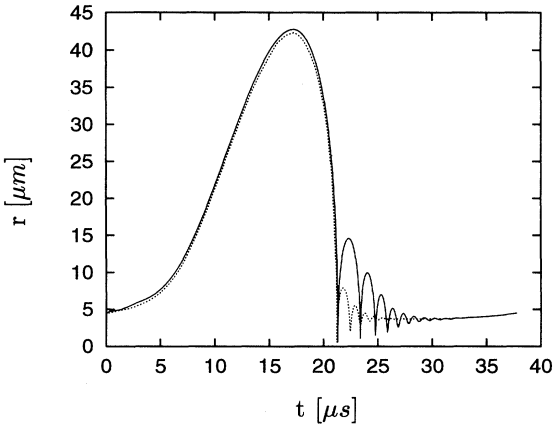

FIG. 1. Bubble radius versus time for one acoustic period. The solid line is the complete solution of Eqs. (3)–(5) combined with Eq. (1). The dotted line is the solution of Eq. (1) assuming adiabatic conditions in the bubble. These are results for an acoustic pressure of 1.325 atm and an initial bubble radius of 4.5 μm (these parameters are used throughout the paper unless specified otherwise). The other parameters entering are acoustic frequency $f_a = 26.5$ kHz, $1/b = 0.794\,\mathrm{g/cm^3}$, $\rho_l = 1.0\ \mathrm{g/cm^3}$, $c_l = 1.481$ km/s, and $\nu_l = 0.01\,\mathrm{cm^2/s}$ (for water at 20 °C). The value of γ in adiabatic solution is 1.4. Surface tension $\sigma = 72.5$ dyn/cm is included.

approximate formula accurately fits the curve for values of R between 1 and 38 μm. As the bubble collapses, however, the influence of the bubble interior becomes more important and it cannot be neglected anymore. It enters into Eq. (1) through the $P_g(t)$ term. Assuming adiabatic conditions in the bubble, $P_g(t)$ follows from the adiabatic equation

$$P_g = P_0 \frac{(R_0^3 - a^3)^\gamma}{(R^3 - a^3)^\gamma} , \tag{2}$$

where R_0 is the equilibrium radius of the bubble, a is van der Walls hard core (for air $R_0/a \sim 8.5$), and γ is the ratio of specific heats. Equations (1) and (2) were solved numerically. We will refer to this solution as an adiabatic solution to the problem. Based on this approach it does not seem to be possible to explain the production of a shock wave in the bubble, as it is not clear if the speed of the bubble wall becomes supersonic with the respect to the speed of sound in the gas. Also, the emission of visible light requires a much higher temperature than that which can be expected based on the adiabatic assumption. So, in order to understand what is really going on in the bubble, especially close to the point of maximum contraction, it is necessary to solve Eq. (1) coupled with the gas dynamics equations.

We assume spherical symmetry for the problem and also neglect the viscosity of the gas and heat conduction. Under these conditions, the gas dynamics equations in the Lagrangian formulation are

$$\frac{\partial V}{\partial t} - \frac{\partial}{\partial \xi}(r^\alpha u) = V^2\,\mathcal{L} , \tag{3}$$

$$\frac{\partial u}{\partial t} + r^\alpha \frac{\partial p}{\partial \xi} = \mathcal{F} , \tag{4}$$

$$\frac{\partial E}{\partial t} + \frac{\partial}{\partial \xi}(r^\alpha u p) = -\Lambda + u\mathcal{F} - p\mathcal{L}V^2 , \tag{5}$$

coupled with

$$\frac{\partial r}{\partial t} = u , \tag{6}$$

which specifies the radial motion of the gas particle. In Eqs. (3)–(5) $V = 1/\rho$ is the specific volume, $E = \epsilon(p,\rho) + u^2/2$ is the energy per unit mass, and $\epsilon(p,\rho)$ determines the equation of state. The variables p, ρ, and u are the pressure, density, and velocity of the gas, respectively. Here α specifies the geometry of the problem, being 0, 1, and 2 for the planar, cylindrical, and spherical cases, respectively. We use $\alpha = 2$ in our calculations. The Lagrangian coordinate ξ and r are related by

$$d\xi = (r^\alpha/V)\,dr = \rho r^\alpha dr \tag{7}$$

or, equivalently, in terms of the initial particle position r_0

$$\rho_0 r_0^\alpha dr_0 = \rho r^\alpha dr. \tag{8}$$

The additional terms that appear in Eqs. (3)–(5) are $\mathcal{L}$, $\mathcal{F}$, and Λ, which represent mass loss, body force, and energy loss, respectively. If the possibility of the gas being dissociated or ionized is excluded (the approximation that is going to be corrected in Sec. II), the equation for the internal energy per unit mass as a function of temperature T is

$$\epsilon(T) = \frac{N}{\gamma - 1} k_B T , \tag{9}$$

which, together with van der Waals equation (without attraction)

$$P\frac{(1 - b\rho)}{\rho} = N k_B T , \tag{10}$$

gives $\epsilon(p,\rho)$, which enters the energy equation (5). Here b is the inverse of the maximum allowed density, N is the number of particles per unit mass, k_B is the Boltzmann constant, and γ is the ratio of specific heats.

The problem of Eqs. (3)–(5) coupled with Eq. (1), which serves as a boundary condition, was solved using a first-order Godunov scheme [11,12]. This method was originally formulated with the goal of establishing a method that retains the simplicity of the method of characteristics. At the same time, it should include the possibility of discontinuous surfaces, such as shock waves and fluid interfaces. In applying the method we divide the region of interest into a number of cells and average the values of the thermodynamic variables in each cell.

The values at the boundaries are calculated using the gas dynamic equations in characteristic form. These boundary values are subsequently used to determine the average values at the later time. The algorithm effectively introduces artificial viscosity, which converts discontinuities common in shock problems into sharp gradients, which permit numerical treatment. [The artificial (kinematic) viscosity introduced is of the order of the grid size multiplied by the sound speed. For a detailed calculation of the shock structure, it is necessary to choose a grid size that would realistically represent the gas viscosity. For our purposes, however, this is not very important.) We varied the number of points in the space grid from 500 to 2000 and the results turned out to be insensitive to the number of points. The time step was determined by the Courant-Friedrichs-Lewy condition and varied from 10^{-8} s for the bubble at maximum radius to 10^{-17} s close to the minimum. The algorithm turned out to be extremely stable.

The results are very sensitive to even small changes of the input parameters, as might be expected for driven nonlinear oscillators. We discuss the influence of changing the parameters later. In Fig. 1 we present typical results for the bubble radius versus time. The results of direct integration of the RP equation (1) (adiabatic solution), for the same parameters, are presented as well. The maximum radius that the bubble reaches is about 42.5 μm at approximately 17.2 μs after the start of the cycle and the minimum is 0.56 μm at about 21.3 μs. For the first part of the cycle, it is easy to see that there is almost no difference in the results between the "adiabatic" solution and the full solution of the system of equations (3)–(5). After the collapse of the bubble starts, however, the motion of the bubble wall becomes faster and when the bubble radius reaches values of a few micrometers it becomes ultrasonic with respect to the speed of sound in the gas. The bubble wall speed and speed of sound in the gas just next to the wall are presented in Fig. 2(b) (for $P_a = 1.325$ atm). At this point a shock wave starts to develop in the bubble and the adiabatic approach is not applicable any more. Figure 3 shows the shock wave propagating in the bubble close to its minimum radius. We should note that the situation presented in this figure

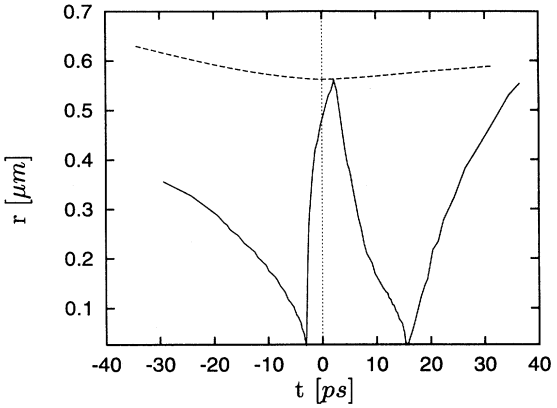

FIG. 3. Shock propagation inside the bubble. (Acoustic pressure of 1.325 atm and initial radius 4.5 μm). For these conditions, the strong shock starts to build up at the point where bubble radius is about 0.8 − 0.9 μm. Time $t_c = 0$ is defined as the time when the bubble wall speed changes sign, which is about 21 μs after the start of the acoustic cycle. The solid line is the shock and the dotted line is the bubble wall.

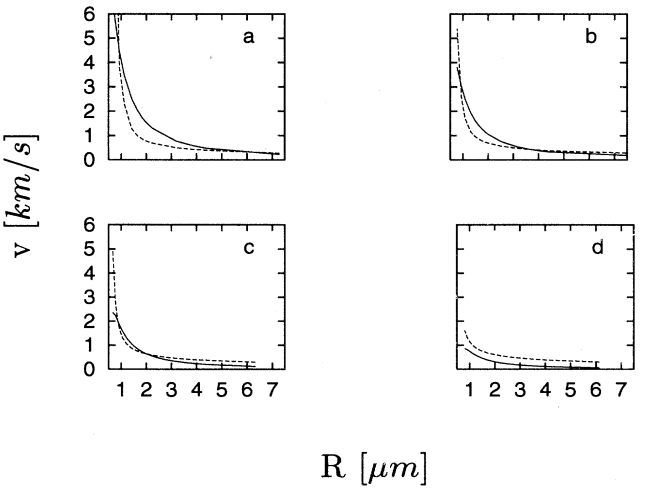

FIG. 2. Bubble wall speed (solid line) and speed of sound (dashed line) close to the minimum radius. For certain acoustic pressure amplitudes, the motion of the bubble wall becomes supersonic with respect to the gas inside the bubble. The bubble radius where that occurs depends on the choice of the acoustic pressure. Here we present results for four different acoustic pressures: (a) 1.425 atm, (b) 1.325 atm, (c) 1.225 atm, and (d) 1.125 atm. The wall motion does not become ultrasonic for the last case.

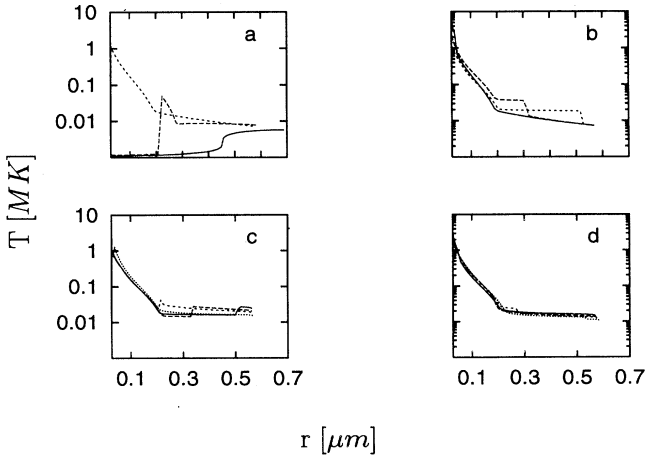

FIG. 4. Spatial profile of the gas temperature at various times close to the time when the bubble achieves its minimum.

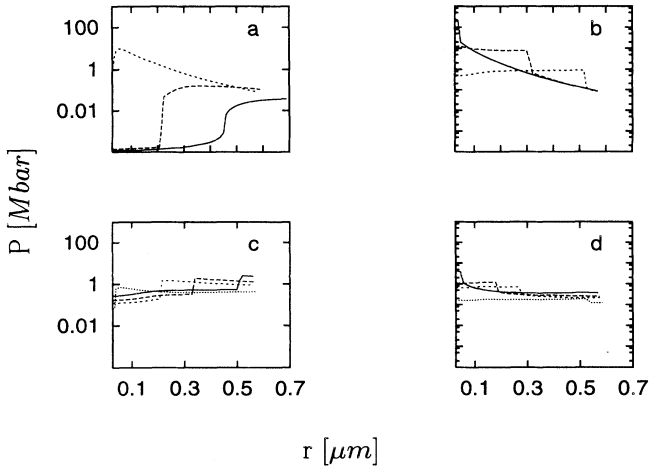

FIG. 5. Spatial profile of the gas pressure at various times close to the time when the bubble achieves its minimum.

represents a solution for the particular choice of parameters that we are using. Different choices of parameters (for example, acoustic pressure or initial bubble radius) lead to different results where more than two shock waves can be present (this result was also reported in [7]) or eventually to just one shock wave.

Results for the spatial profile of the thermodynamic variables as the solution of Eqs. (3)–(5) coupled with Eq. (1), in which loss terms have being neglected, are presented in Figs. 4–6. These results are similar to those given in [5,6]. In Fig. 4(a) the shock is moving inward (the curves are for $t = t_c - 49.6\,\text{ps}$, $t_c - 13.5\,\text{ps}$, and $t_c - 3.1$ ps, where time t_c is defined as the time when the bubble wall velocity changes sign). In Fig. 4(b) the shock rebounds and propagates outward and hits the wall at about 2 ps after t_c (the curves are drawn for $t = t_c - 3.0\,\text{ps}$, $t_c - 2.3$ ps, and $t_c + 1.0$ ps). In Fig. 4(c) it reflects from the wall and collapses again (the curves are drawn for $t = t_c + 3.0\,\text{ps}$, $t_c + 5.6\,\text{ps}$, $t_c + 8.2$ ps, and $t_c + 15.3$ ps). In Fig. 4(d) the shock rebounds after the second collapse and propagates outward (the curves are drawn for $t = t_c + 16.2\,\text{ps}$, $t_c + 19.9\,\text{ps}$, $t_c + 22.4$ ps, and $t_c + 34.5$ ps). Note the huge temperatures developing close to the bubble center. The propagation of the shock could be easily followed in Figs. 5 and 6 as well.

Later we are going to compare some of these results with those following from the solution of Eqs. (3)–(5) where the loss terms are included. The inclusion of these loss terms is the subject of the next section.

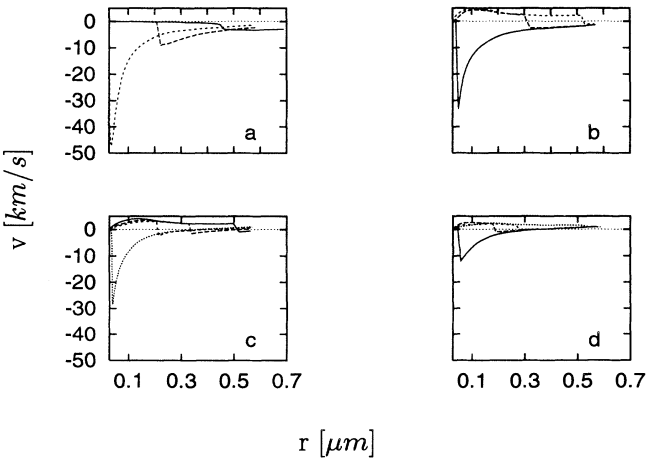

FIG. 6. Spatial profile of the gas velocity at various times close to the time when the bubble achieves its minimum.

II. INCLUSION OF THE LOSS TERMS

The results of integration of Eqs. (3)–(5) without loss terms imply the existence of extreme conditions in the bubble center during the shock collapse. Theoretical temperatures as high as 10^7 K and pressures on a megabar scale have been reported [5–7]. These results would imply that some very energetic processes, including nuclear fusion, might occur in the bubble close to the origin, as pointed out in [8]. These results also imply that mechanical energy losses may also be considerable. Inclusion of these terms is important in order to make a self-consistent prediction of the real temperatures that develop in the center of the bubble during the shock collapse(s). Finally, they are responsible for the effect of SL, which we want to explain. These loss terms include the following processes: heat flow between the bubble and liquid, thermal conduction in the gas, inclusion of vibrational degrees of freedom in the equation of state, dissociation of the gas, ionization of the gas, and radiation losses that are responsible for the effect of SL.

The first two effects are definitely important in order to completely understand the general bubble dynamics and the remarkable stability of the bubble oscillations, as pointed out in many references [13–21]. Their discussion, based on simple mechanical arguments, is given in Appendixes A and B. The conclusion is that these effects do not have an important influence on the gas dynamics on the time scale of interest. This time scale (a few tens of picoseconds) is determined by the time which the bubble spends close to its minimum radius, shock waves are produced, and the SL pulse emitted. In the rest of this section we explain how the rest of the above mentioned processes should be included in order to get a more complete understanding of the gas dynamics. Some details are presented in Appendixes C–F. The discussion of the relative importance of various energy loss mechanisms will be presented in Sec. III.

The effect of the inclusion of vibrational degrees of freedom and dissociation is mainly in the change of the equation of state. Dissociation also leads to certain energy losses, which were included in Eq. (5). Two questions relate to ionization. First, is there a kinetic pathway open to initiate the ionization? Second, is thermal equilibrium established between the electrons and ions?

For now we assume that the answer is "yes" to both of these questions. Then the Saha equation is applicable (see Appendix C). We defer further remarks to Sec. III. An important point about the ionization of the gas is that at the temperatures that are of interest to us (10^5 K or more), multiple ionization can take place, which leads to mechanical energy loss and also to a significant change in the optical properties of the bubble. Equalization of electron and ion temperatures occurs after many collisions due to the large difference between the electronic and ionic masses. The approximate result for this time is [22]

$$\tau \sim \frac{m}{m_e} \frac{1}{N \overline{v}_e \sigma} , \tag{11}$$

where m is the ionic mass, m_e is the electron mass, N is the ion number density, $\overline{v}_e$ is the mean electron velocity, and σ is the cross section for electron-ion collisions. For typical values of the parameters entering our problem, i.e., $T \sim 10^5$ K, $N \sim 10^{22}\,\mathrm{cm}^{-3}$, the result for τ is of the order of $10^{-13} - 10^{-12}$ s . This is still short compared to the time bubble spends close to the minimum. This means that the translational temperature is established rather fast and that ions and electrons could be assumed to be at the same temperature.

The self-consistent inclusion of radiation into the gas dynamics equations is explained in Appendixes D and F. We present two radiative mechanisms. The "thermal approach" is based on the coupling of radiative transfer equation with the gas dynamics equations. Let us emphasize that the resulting radiation is not *a priori* related to blackbody radiation. An object is going to radiate as a blackbody if it is optically thick ($d \gg l_a$), where d is the typical dimension of the object and l_a is the radiation absorption length. It will radiate as a volume radiator if it is optically thin ($d \ll l_a$). The radiative transfer equations (based on the principle of detailed balance) is a complicated problem in itself. Correspondingly, a number of approximations have to be made in order to efficiently couple this equation with the gas dynamic equations (for details, see Appendix D). The important factor that enters into the radiative transfer equation is the radiation attenuation coefficient. In general it is very difficult to calculate this quantity in an exact manner since there are many processes that are involved. The overview of the different processes that are important in getting approximate results for the attenuation coefficient under the extreme conditions in the bubble close to its minimum radius is given in Appendix E. Here we note that a crucial factor which has a big influence on the results for the attenuation coefficient is multiple ionization, discussed above. Some representative values are given in Table I. The strong temperature and frequency dependence of the absorption coefficient κ'_ν should be noted. For high temperatures (more than 10^6 K) the values for the absorption coefficient are very high, giving very short radiation mean free paths. For lower temperatures the values of the absorption coefficient are smaller, giving radiation mean free paths that are comparable to the bubble size (or larger). This means that the absorption of radiation in the bubble is going to be important, especially for the high temperatures near the bubble center.

TABLE I. Values of absorption coefficient κ'_ν and average ionization $\overline{m}$ for a few temperatures T and angular frequencies of radiation ω. These results are for a density of the gas equal to $0.7\,\mathrm{g/cm}^3$.

T(K)	ω (s^{-1})	$\overline{m}$	κ'_ν (1/cm)
2.5×10^4	5.0×10^{15}	0.025	3.0×10^3
5.0×10^4	5.0×10^{15}	0.20	5.1×10^4
1.0×10^5	5.0×10^{15}	0.64	3.6×10^5
1.0×10^6	5.0×10^{15}	5.0	3.1×10^5
2.0×10^6	5.0×10^{15}	6.7	2.2×10^6
1.0×10^7	5.0×10^{15}	7.0	5.7×10^7
1.0×10^5	1.0×10^{15}	0.64	7.6×10^6
1.0×10^5	5.0×10^{15}	0.64	3.6×10^5
1.0×10^5	1.0×10^{16}	0.64	1.1×10^5
1.0×10^5	5.0×10^{16}	0.64	7.9×10^4
1.0×10^5	1.0×10^{17}	0.64	1.0×10^4
1.0×10^5	5.0×10^{17}	0.64	8.1×10^1
1.0×10^5	1.0×10^{18}	0.64	1.1×10^1
1.0×10^5	1.0×10^{19}	0.64	1.0×10^{-2}

The other approach to the radiation problem is based on bremsstrahlung (Appendix F). We may think of bremsstrahlung as radiation emitted due to the sudden changes of microscopic "dipole" moments associated with the collision process. Since the temperatures close to the center of the bubble at the time of the complete collapse of the shock waves reaches values of a few million degrees, one could expect the formation of a plasma. This means that bremsstrahlung happens in the "ball" of plasma and one has to include the corrections to individual scattering events due to the rest of the plasma. We approximate the plasma in the bubble center as being uniform, which allows us to formulate a simple model for the calculation of the corrected bremsstrahlung radiation.

III. DISCUSSION OF THE RESULTS

First, let us study the relative importance of the various mechanisms for energy loss. The most important changes result from the inclusion of radiation. It is necessary in order to have the theory consistent with the law of conservation of energy. As the core of the bubble is heated by the collapsing shock wave it reaches a high temperature (which in the absence of radiation would, in fact, become infinite, as shown by Guderley [23]). The radiation of energy serves to limit this heating since the hotter the core gets the more energy it radiates. It is of crucial importance to include this "radiation reaction" in a self-consistent way because the reduction of energy in the core lowers the pressure and modifies the dynamics. Thus the mechanical motion and the radiation are intimately connected. Previous descriptions of the problem [5–7] computed the radiation as a consequence of the dynamical motion but did not include the feedback on the mechanics. Those theories obtained a serious overestimate of the core temperature. The self-similar solution to the gas dynamic equations in the absence of the loss

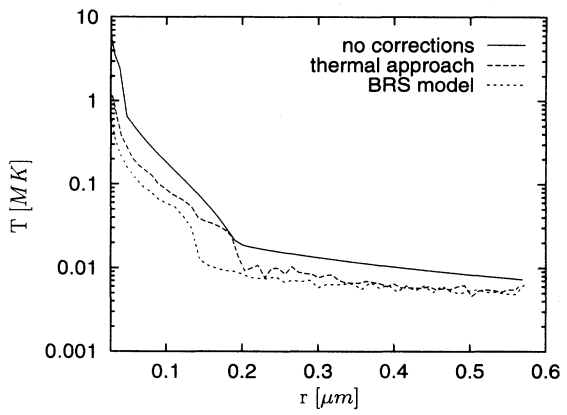

FIG. 7. Spatial profile of the gas temperature at the time immediately after the first shock rebounds from the origin for different methods of introducing energy losses. BRS denotes the bremsstrahlung model.

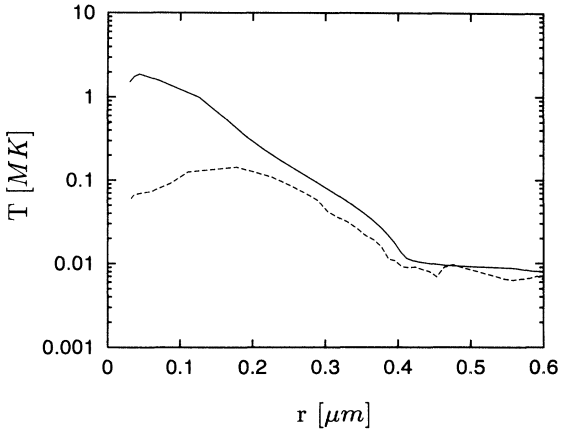

FIG. 8. Temperature in the bubble about 200 ps after collapse of the first shock. The solid line represents the solution without the inclusion of loss terms. The broken line is the solution if all energy-loss mechanisms are included (the thermal model is used here).

terms leads to the singularity in $T(t)$ when the shock wave collapses to the origin. Inclusion of the loss terms tempers this singularity. The physics is simple: as $T(t)$ rises so does the thermal emission. The system cools off. Energy conservation therefore keeps $T(t)$ finite over any finite region of space. Furthermore, a numerical treatment of the singular problem might have been dependent on the grid size used in the calculations. These problems are avoided by the self-consistent calculation performed here.

Results for the temperature close to the origin during the shock collapse are presented in Fig. 7. One can easily verify that the maximum temperature close to the origin is about an order of magnitude smaller than the results without corrections. A very important point about the inclusion of losses (especially radiation losses) is that it provides a natural mechanism for cooling of the bubble. To illustrate this point we present in Fig. 8 the results for the temperature in the bubble at a time about 200 ps after it achieves its minimum radius. We can see that there is a big difference in the results, especially close to the bubble center. Here the thermal approach is used for inclusion of radiation losses. The bremsstrahlung approach leads, however, to similar results for the temperature and pressure. The influence of radiation and other losses on emission of radiation in the form of a SL pulse is going to be discussed in Sec. IV.

Let us now discuss the influence of the change of some of the parameters on the results for the thermodynamic variables. The results for the pressure and temperature in the bubble after the first shock rebounds from the origin are shown in Figs. 9 and 10 for different acous-

TABLE II. Expansion ratio R_m/R_0, maximum velocity of the bubble wall v_m, radius at which the bubble wall becomes ultrasonic R^{ultra}, number of photons N_p emitted in the SL pulse, and average power $\overline{P}_a$ emitted during 10 ps around the maximum of the power output are presented for different acoustic pressures P_a and equilibrium radii R_0.

P_a (atm)	R_0 (μm)	R_m/R_0	v_m (km/s)	R^{ultra}/R_0	N_p	$\overline{P}$ (mW)
1.425	4.50	12.8	6.0	1.44	8.2×10^6	5.5×10^2
1.375	4.50	11.7	5.3	1.11	3.0×10^6	3.0×10^2
1.325	4.50	10.6	3.9	0.80	2.2×10^6	1.4×10^2
1.275	4.50	9.4	3.1	0.62	6.7×10^5	4.2×10^1
1.225	4.50	7.9	2.2	0.41	1.1×10^5	6.6
1.175	4.50	7.1	1.6		very small	very small
1.125	4.50	5.8	0.9			
1.325	10.0	5.8	2.13	0.25	2.4×10^6	1.6×10^2
1.325	6.00	8.4	3.51	0.55	5.2×10^6	3.4×10^2
1.325	4.50	10.6	3.94	0.76	3.0×10^6	3.0×10^2
1.325	3.75	12.4	4.24	0.80	1.4×10^6	9.0×10^1
1.325	3.00	14.9	4.34	1.00	5.2×10^4	3.1×10^{-1}

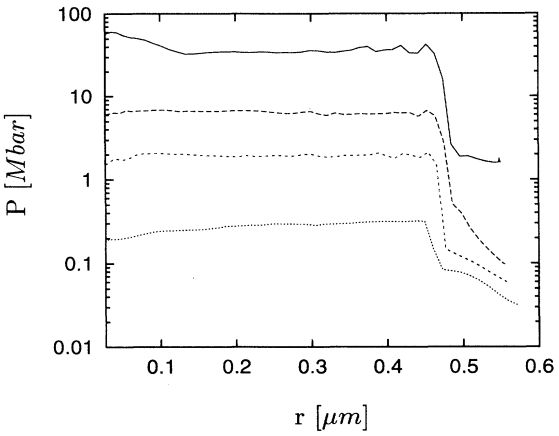

FIG. 9. Pressure in the bubble for various acoustic pressures immediately after the first shock rebounds from the origin. The results are for acoustic pressures of 1.375 atm (solid line), 1.325 atm (long-dashed line), 1.275 atm (short-dashed line), and 1.225 atm (dotted line).

tic pressure amplitudes. We see that a change of 10% in driving pressure produces a difference of about two orders of magnitude for the temperature close to the origin and even more for the pressure. The explanation for these drastic changes can be found in Fig. 2 (see also Table II). From Table II we see that for higher acoustic pressures the ratio R_m/R_0 is large. This leads to faster collapse of the bubble wall. It achieves supersonic speed with respect to the gas inside the bubble while the bubble is still relatively large (6.5 μm for acoustic pressure of 1.425 atm). Thus stronger shock waves are produced, which leads to huge temperatures and pressures in the bubble. On the other hand, if the acoustic pressure is not high enough [see Fig. 2(d)], the motion of the bubble wall never becomes ultrasonic. The conditions for formation of a shock wave are not fulfilled and conditions in the bubble are almost adiabatic and, of course, there is no SL radiation). The influence of different acoustic pressure amplitudes on the motion of the bubble wall close to the minimum radius can be seen in Fig. 11. We see that for acoustic pressures above some threshold value (about 1.2 atm), the minimum bubble radius is almost independent of it (for the initial bubble radius of 4.5 μm this minimum radius is about 0.55 μm). A higher acoustic pressure results in a faster collapse of the bubble wall, as already noticed. But, if the acoustic pressure is not high enough (for example, $P_a = 1.175$ atm in Fig. 11), the minimum bubble radius is larger and the collapse is much slower. Later we are going to see that this threshold value of acoustic pressure also represents the minimum pressure that still leads to the emission of a SL pulse.

Concerning the influence of a different initial bubble radii, the conclusion is not so simple. It seems that there are two competing effects taking place. On the one hand, from Table II we can see that smaller bubble expands more (the R_m/R_0 ratio gets larger for smaller R_0), so the collapse of the smaller bubbles should be faster. This leads to an earlier production of the shock wave and stronger collapse. On the other hand, in initially very small bubbles ($R_0 \sim 3.0\,\mu$m), the shock wave is produced close to the center, so it does not develop very high temperatures during the final stages of its collapse. For initially large bubbles ($R_0 \sim 10\,\mu$m), the situation is opposite. The bubble does not grow very much during the expansion part of the cycle, so the collapse is weaker. That leads to the production of a weaker primary shock wave and lower temperatures in the bubble center. We will see the influence of the initial bubble radius on the emission of SL pulses in Sec. IV.

One of the interesting consequences of an initially small bubble radius is that the shock wave is produced relatively early, so the rebounded wave hits the bubble wall while it is still moving inward. The result is an even stronger rebound. The rebounded wave hits the origin

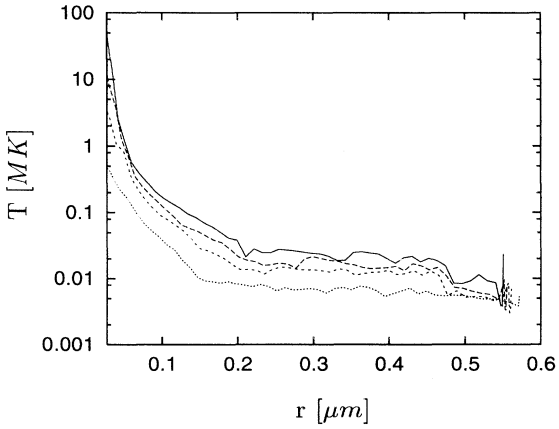

FIG. 10. Temperature in the bubble for various acoustic pressures immediately after the first shock rebounds from the origin. Acoustic pressure amplitudes are the same as in Fig. 9.

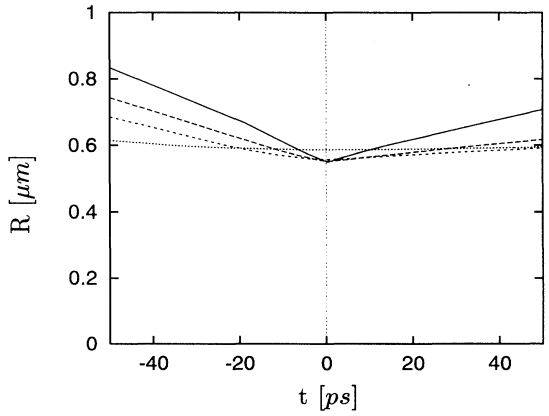

FIG. 11. Bubble radius close to its minimum for various acoustic pressures. The solid line is for $P_a = 1.425$ atm, the long-dashed line is for $P_a = 1.375$ atm, the short-dashed line is for $P_a = 1.275$ atm, and the dotted line is for $P_a = 1.175$ atm.

again, rebounds, and reaches the bubble wall one more time. For the case of $R_0 = 3.0\,\mu$m we were able to count at least five of these rebounds. As the rebounded waves become weaker, the temperature and pressure gradients are not as strong as for the first one.

IV. SONOLUMINESCENT RADIATION

In the previous sections we presented two approaches to the problem of radiation energy loss. The same mechanisms are going to be responsible for the emission of a SL pulse. The main difference between these two approaches is in how to treat the small region around the bubble center where the temperature is very high.

In the thermal model, we think about the bubble as a miniature "sun." Both systems contain a hot core, which is optically thick (cf. Table I), surrounded by a much cooler envelope. The fact that the system is small leads to corrections, but the basic fact is still there: the outer envelope, and not the core region, is responsible for the radiation that is seen in experiment [3]. The spectrum that we finally get is not a pure blackbody spectrum since it represents a superposition or radiative contributions from the entire plasma, corrected for the absorption effects. Nevertheless, one may loosely characterize it as an effective blackbody characterized by the temperature in the envelope region (20 000-30 000 K) since this region is the most important factor in determining the spectral properties of emitted radiation (see below). The actual calculation of SL pulse is based on the result for energy loss (D2), with the frequency integration modified in order to account for the absorption in the water. The importance of the inclusion of radiation loss terms in the treatment of the gas dynamics equations can be seen in Fig. 12. There is not much difference in the power emitted until the collapse of the first shock (at a time about 3 ps before t_c, defined as the time when bubble wall velocity changes sign). At this point, however, a lot of energy is radiated and the temperature becomes much smaller than it did in the uncorrected solution. The second peak in the power spectrum of the uncorrected solution corresponds to the collapse of the second shock wave. We conclude that inclusion of loss terms, especially radiation, is very important in order to explain the SL pulse. It also explains the short duration of the pulse (in the uncorrected solution, the SL pulse lasts much longer; cf. Fig. 12. Our results imply that the duration of the pulse is about 10 ps, shorter than 50 ps, which is the current experimental upper bound [2].

It is important to note that the effect of SL cannot be explained based on pure bremsstrahlung, since the spectral power of bremsstrahlung radiation falls with increasing frequency instead of rising as seen in experiment [3]. Our bremsstrahlung model represents the extension of simple bremsstrahlung radiation in the sense that we account for the frequency-dependent absorption of radiation in a region around the plasma and for the corrections to individual bremsstrahlung events due to the presence of the rest of the plasma (cf. Appendix F). The peak power emitted in the form of SL pulse resulting from this approach is similar to the one from thermal approach and the duration of the pulse is a little longer. The results for the spectrum of the emitted radiation are given in Fig. 13. We see that the spectral properties that result from the thermal approach (fairly close to the Planck spectrum with a temperature of 25 000 K) are in much better agreement with experimental results, so it seems that this approach better explains the physical processes in a sonoluminescing bubble.

The results for some important quantities that determine the radiation coming out of the bubble are sum-

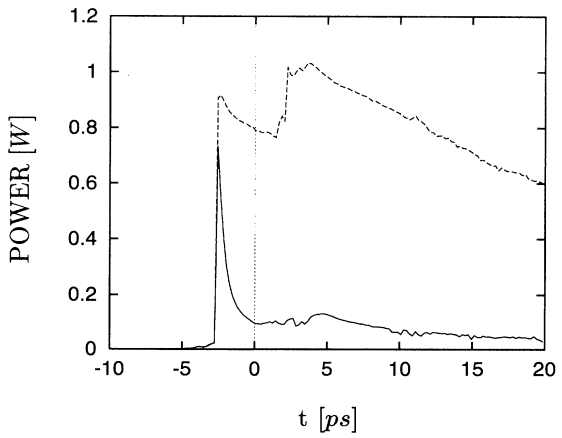

FIG. 12. Power versus time for the SL pulse. Results with inclusion of all loss mechanisms (solid line) and without inclusion of radiation losses (broken line) are presented.

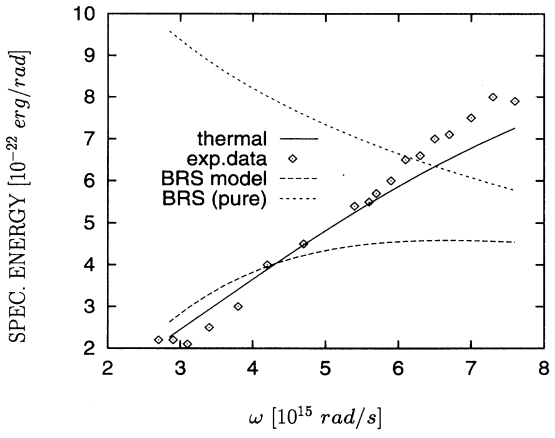

FIG. 13. Spectrum of emitted SL radiation resulting from the thermal and bremsstrahlung approach. The "pure" bremsstrahlung results are obtained without corrections due to the presence of a plasma and absorption. The acoustic pressure amplitude is 1.325 atm for both the theoretical and experimental results. The attenuation of radiation in the water and the container walls was not taken into account. The theoretical results were scaled down to the experimental ones.

marized in Table II. Clearly, higher acoustic pressure amplitudes lead to higher bubble wall speeds, so the shock waves are produced sooner and their collapses are stronger. This leads to higher temperatures in the bubble and more radiative energy output. This is also illustrated in Fig. 14. The peak power for the experimental conditions [3] is about 100 mW, consistent with the experimental lower limit of 30 mW [3]. (The absorption of radiation in water or container walls was not taken into account in our approach.) The sharp rise and slower decay of the pulse, which were observed experimentally [2], can be noticed as well. The other interesting result of our theory follows from the observation that the temperatures in the center of the bubble get to be very high if the bubble is driven with high acoustic pressure (cf. Fig. 10). We can see in Table I that for the high frequencies (10^{18} rad/s or more), the absorption coefficient is very small, thus the bubble is optically thin. That means that the emission of x rays could be expected if the temperatures in the center of the bubble really reach values of the order of 10^8 K. Since the absorption length of x rays is fairly long in the water as well, this effect should be observable. It could also give us the answer as to how hot the bubble center really is. We emphasize that, as a result of our theory, this effect should be expected only for very strongly driven bubbles, with acoustic pressure amplitudes of at least 1.4–1.5 atm. However, it is not clear that the bubble will remain dynamically stable when it is driven so strongly since it is close to its upper stability threshold. The bubble could be destabilized by the growth of aspherical modes of oscillations. We leave it to experiment to determine the range of stability of the bubble.

Concerning the influence of the initial bubble radius on the SL radiation, we have already seen in Sec. III that there are two competing effects taking place. The net result is that the sonoluminescent emission is largest for some intermediate values of the equilibrium bubble radius. The SL power outputs for different initial bubble radii are presented in Fig. 15. Here one should take cognizance of the 5–10 % uncertainty in the experimental results for the equilibrium bubble radius [8]. This uncertainty limits the comparison of our results with experiment.

The spectrum of the emitted radiation is presented in Fig. 16. We show the experimental data and our results for a few acoustic pressure amplitudes. Note that higher acoustic pressure amplitudes lead not only to more power output but they also change the frequency dependence of the spectral power. If one wants to fit the emitted spectrum to a blackbody spectrum, the conclusion would be that the radiation from the bubble exposed to a higher acoustic pressure field corresponds to a higher "blackbody" temperature.

Finally, we would like to comment on one of the most intriguing facts about SL radiation, i.e., the strong dependence of SL intensity on water temperature. SL radiation increases more than ten times if the liquid is cooled down to freezing point [3]. Our approach treats the bubble-liquid interaction very approximately (through the RP equation), but we hope that we can indirectly understand this striking observation. First, as noticed in [3], the water dissolves about twice as much air at 0 °C compared to 20 °C. The mass flow between the bubble and water is important in stabilizing the bubble oscillations through longer periods of time [8]. One could expect that more air from the water is going to evaporate into the bubble if the concentration of the dissolved air in the liquid next to the bubble is higher (following Henry's law, the partial pressure in the gas is proportional to the concentration in the liquid). The conclusion is that one could expect more air in the bubble in a colder liquid or, correspondingly, a larger bubble. If the bubble is initially small (for example, 3 μm), this flow of air between the wa-

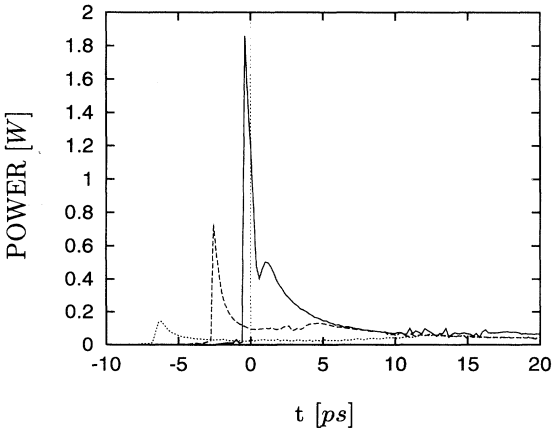

FIG. 14. SL emission for various acoustic pressures. The full line corresponds to 1.375 atm, the dashed one to 1.325 atm, and the dotted one to 1.275 atm. The results for lower acoustic pressure amplitudes are out of scale.

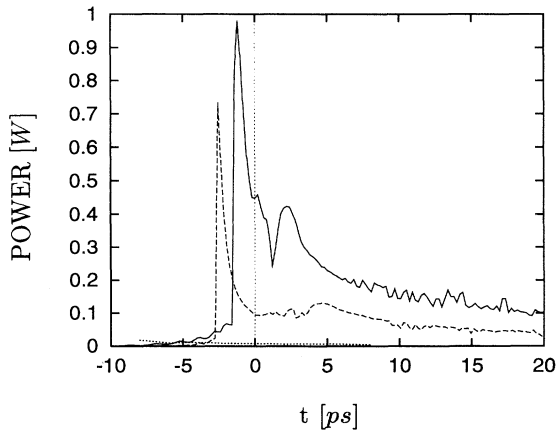

FIG. 15. SL emission for various initial bubble radii. The full line corresponds to $R_0 = 6.0\,\mu$m, the dashed one to 4.5 μm, and the dotted one (barely visible) to 3.75 μm.

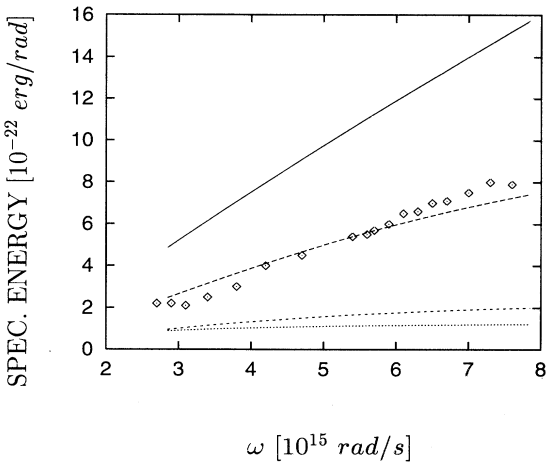

FIG. 16. Spectrum of emitted SL radiation. Squares are experimental data, lines correspond to acoustic pressures of 1.375 atm (solid line), 1.325 atm (long-dashed line), 1.275 atm (short-dashed line), and 1.225 atm (dotted line). Theoretical results were scaled down to experimental values. The attenuation of the radiation in the water and in the container walls (see [24]) was not taken into account in the theoretical results.

ter and bubble might have considerable influence. From Table II we can see that a 3.75 μm bubble produces more than an order of magnitude more radiation than a 3.0 μm bubble. Since mass diffusion is a slow process, the time delay for the emission of SL pulse, reported in [8], can be explained as well. On the other hand, it seems [8] that the experiments with water at lower temperatures were done with higher acoustic amplitudes. That would also increase the SL emission, as pointed out earlier. Also, the SL pulse from the cold liquid was fitted to a higher black body temperature [3]. This corresponds to our observation that the SL spectrum fits to higher temperatures if the acoustic pressure is increased.

One of the curious features of SL experiments has been the role played by rare-gas additives. It seems that [24] some rare-gas is needed to produce SL. The precise origin of this effect is not yet understood. Penning ionization has been conjectured [24] as possibly being involved, although no details have been provided. One possibility is that the rare gas may be responsible for promoting the initial ionization of the molecular gas by a collisional ionization process. This could come about as follows. When the gas is imploded and the temperature is raised, the rare gas has some probability for being collisionally excited into a metastable state. This would occur in the core of the bubble near the point of collapse of the shock wave where the kinetic energy is high. Metastable states exist for all the rare gases. Thus Ne, Ar, Kr, and Xe have metastable triplet $^3P_0$ and $^3P_2$ states. Helium has, in addition, long-lived $^3S_0$ and $^1S_0$ states. The lifetime of the metastable states is expected to be very long since they are forbidden to decay by multiple selection rules. The metastable states are likely to persist for many oscillations of the bubble and therefore a slow buildup of their population will occur from cycle to cycle. As the metastable population builds up, the onset for electron ionization will occur earlier in the bubble collapse phase. Following initial ionization, further ionization will progress by electron avalanche ionization, where the electron population grows exponentially. The rare gas may therefore serve as a catalyst in promoting the initial stage of ionization of the gas. This may account for the fact that it often takes many oscillations of the bubble before SL is produced. Metastable states may also promote competitive processes, such as the dissociation of the molecular gas.

In our theory, we have assumed that the ionization process occurs (by whatever means) and have used the Saha equation to give the density of electrons to be expected. The Saha equation is based on thermodynamic equilibrium. The avalanche process involves the exponential growth of the number of electrons so once a single free electron is produced, rapid growth in the electron number ensues and the electrons equilibrate.

One possible way to test the above hypothesis is to take a pure molecular gas (without rare-gas additives) in a contracting bubble and expose it to ionizing radiation. If free electrons are produced and electron avalanching ensues, it could mimic the hypothesized seeding effect of the rare gas.

Other explanations for the role played by rare gases may involve the stability of the bubble itself. It is not yet understood how the exchange of mass and/or heat with the surrounding liquid influences the change in the equilibrium size of the bubble and how that affects its stability. One may ask if the admixture of rare gas serves to regulate this exchange. In our theory we have bypassed these intriguing questions and assumed that the bubble is stable, in local thermodynamic equilibrium, and is radiating SL. The parameters of our theory are the equilibrium bubble radius and the acoustic pressure amplitude. These are both obtainable, in principle, from experiment.

CONCLUSION

Our formulation of the physics of a collapsing bubble in a liquid provides an improved approach to the sonoluminescence problem. A self-consistent calculation of the bubble dynamics, coupled with radiative transport, is necessary in order to obtain reasonable results for the gas properties and to explain the sonoluminescent radiation. The duration of the SL pulse, the spectral properties, and the strong dependence of the SL pulse on parameters that were reported experimentally [8] are explained from a theoretical point of view. The maximum temperature in the bubble is strongly dependent on the acoustic amplitude and might reach values of tens of millions of degrees, provided the imploding shock wave remains stable until very close to the bubble center. At this point, however, our approach does not take into account mass diffusion since we are concerned with the steady state regime of bubble motion. A more complete theory, which would account for the precise chemical nature of the gas

in the bubble and remove some of the uncertainties of the current model, will be possible when more experimental data are available. For the time being, the process of mass diffusion, which is important in this sense, is not well understood. Finally, the formulation of a more complete theory is needed in order to understand some recent experimental results, such as the strong dependence of the SL radiation on doping with inert gases [24]. We believe that our approach gives a good starting point in that direction.

APPENDIX A: HEAT FLOW BETWEEN THE BUBBLE AND LIQUID

We want to estimate the importance of heat conduction between the gas in the bubble and liquid during the final stages of bubble collapse. We provide here an estimate of the upper limit of the amount of energy that can be transferred.

The heat transferred per time is given by

$$\dot{Q} = N_c C_v \Delta T \frac{1}{N_a} , \tag{A1}$$

where N_c is number of collisions of gas molecules with the bubble wall per unit time, C_v is molar heat capacity, ΔT is the temperature difference between the gas and liquid, and N_a is Avogadro's number. Equation (A1) overestimates the heat transfer since it assumes that all available energy is transferred in the collisions. The number of collisions follows from the estimate of the total momentum transferred to the wall during the time Δt because of the collisions $\Delta P/\Delta t \sim 2m\overline{v}/3\,N_c$, where m is molecular mass and $\overline{v}$ is the average thermal velocity of molecules. By equating the total momentum transferred in the time interval Δt with the average force, which is in turn equal to the pressure exerted on the bubble wall multiplied by area, we get a final estimate for heat transferred per unit time

$$\dot{Q} \sim \frac{15}{4}\left(\frac{k_B N_a}{3MT}\right)^{1/2} AP\Delta T . \tag{A2}$$

Here P is the pressure in the bubble, A is the area of the bubble, M is the molar mass of the gas in the bubble, and k_B is Boltzmann's constant. Typical values of the variables entering Eq. (A2) for the bubble close to the minimum radius are $P \sim 10^{11}\,\mathrm{dyn/cm^2}$, $A \sim 4.5 \times 10^{-8}\,\mathrm{cm^2}$, and $\Delta T \sim 10^4$ K. (We assume that the liquid is at room temperature. This assumption overestimates the transfer of heat since the liquid next to the bubble wall is heated as well.) This gives $\dot{Q}\Delta t \sim 7 \times 10^8 \Delta t$ ergs/s. This value should be compared with the typical value of the total energy in the bubble E_T, given by Eq. (9) multiplied by bubble mass. For $\rho \sim 0.5\,\mathrm{g/cm^3}$ and a bubble mass of approximately 5.5×10^{-12} g we get $E_T \sim 1$ erg. For the time $\Delta t \sim 100$ ps, the upper limit on the heat transferred between the bubble and the liquid is about 0.07 erg. We conclude that at most a few percent of the energy of the gas could be expected to transfer to the liquid, so the effect of heat transfer between the bubble and the liquid does not have an important effect, at least not for the short time that the bubble spends close to its minimum radius.

APPENDIX B: HEAT CONDUCTION IN THE GAS

One of the assumptions in our study of shock propagation is that heat conduction in the gas can be neglected. Let us estimate the importance of this effect for the time scale at which shock wave(s) actually exists: about $50 - 100$ ps. The flow of heat is given by the heat conduction equation

$$\frac{\partial T}{\partial t} = \chi \nabla^2 T , \tag{B1}$$

where the coefficient of thermal diffusion is given by $\chi = l_a \overline{v}/3$. Here l_a is molecular mean free path and $\overline{v}$ is the average molecular thermal speed. For standard values of temperature T and number density n_s the value of χ is about $0.2\,\mathrm{cm^2/s}$ [22]. Noting that l_a is inversely proportional to the density of the gas n and $\overline{v}$ is proportional to $T^{1/2}$, when the shock is close to complete collapse ($n \sim 500\ n_s$ and $T \sim 10^5$ K), we get a value for $\chi \sim 6 \times 10^{-3}\,\mathrm{cm^2/s}$. From Eq. (B1) we see that the time Δt required to equalize the temperature across distance Δx is given approximately by

$$\Delta t \sim \frac{(\Delta x)^2}{\chi} . \tag{B2}$$

For a typical distance of 10^{-5} cm, the time required is a few nanoseconds. This is very long compared to the typical lifetime of the shock waves, so we conclude that the effect of heat conduction in the gas is not important in our problem.

APPENDIX C: VIBRATIONAL DEGREES OF FREEDOM, DISSOCIATION, AND IONIZATION

The temperature at which the vibrational degrees of freedom unfreeze is on the order of a few thousand degrees. As we are mainly interested in much higher temperatures (10^4 K or more), we included this effect simply by changing the ratio of heat capacities from 7/5 to 9/7 for temperatures higher than "critical" ones. The critical temperature was taken to be 4×10^3 K. This choice does not have much influence on the final results. The same is true for the choice of temperatures that govern the process of ionization and dissociation mentioned below.

The dissociation of air starts at temperatures of the order of 10^4 K [22]. The energies required for dissociation are considerable, 5.11 eV for O_2 and 9.74 eV for N_2 [25]. The equation of state becomes

$$\epsilon(T) = \frac{N}{\gamma_m - 1}[1 - \alpha(T)]k_B T + 2\frac{N}{\gamma_a - 1}\alpha(T)k_B T + N\alpha(T)U \ , \quad \text{(C1)}$$

where $\alpha(T)$ measures the degree of dissociation [$N\alpha(T)$ molecules are dissociated] and U is the dissociation energy. Here γ_m is the molecular ratio of heat capacities (9/7 for air if the vibrational degrees of freedom are included) and γ_a is the monoatomic ratio (5/3). The first term on the left-hand side of Eq. (C1) corresponds to the energy of molecules, the second one to the energy of the atoms, and the last one represents the energy required for dissociation. Since our treatment is approximate, we used statistically averaged values for the dissociation energies of O_2 and N_2 mentioned earlier. This last term was included in Eq. (5) as a mechanical energy loss. As in the case of the vibrational degrees of freedom, we are not interested in the details of the dissociation process. Hence a simple linear model was employed for $\alpha(T)$:

$$\alpha(T) = \frac{T - T_{D1}}{T_{D2} - T_{D1}} \ , \quad \text{(C2)}$$

where T_{D1} and T_{D2} are temperatures at which dissociation starts and ends (taken as 5×10^3 K and 10^5 K), respectively. The relaxation time for dissociation for conditions such as ours (high temperature and density) is of the order of 10^{-12} s [22], which is fairly short compared to the time the bubble spends close to the minimum radius. That means that there is enough time for equilibrium to be established. Finally, the net result of dissociation is that the number of particles per volume increases from N to $[1 + \alpha(T)]N$ and there is a mechanical energy loss mechanism, which is to be included in our gas dynamics equations.

Inclusion of ionization into the gas dynamics equation is more complicated. Ionization in air starts at temperatures of about 10^4 K, but already at temperatures of few times this value there is a considerable number of double and triply ionized atoms. The ionization process at equilibrium is governed by the Saha equation, which becomes complicated to use if there is multiple ionization taking place. To simplify things, we employ a continuous approximation that gives the average degree of ionization $\overline{m}$ (the number of electrons per initial atom or molecule). Namely, the Saha equation gives a system of recurrence relations for the number of ions with degree of ionization m. By replacing finite differences in the Saha equation by differentials and using conservation of the number of particles and of the total charge, the following transcendental equation is obtained:

$$I(\overline{m} + 1/2) = k_B T \ln \frac{AT^{3/2}}{\overline{m}n} \ , \quad \text{(C3)}$$

where $I(\overline{m} + 1/2)$ is given by a continuous curve constructed by joining the points I_m corresponding to ionization potentials for ionization of degree m. In Eq. (C3) n is the number of atoms (molecules) per unit volume, T is the temperature, and A is the constant coming from the Saha equation $A = 2(2\pi m_e k_B/h^2)^{3/2}$. By solving Eq. (C3) we obtain $\overline{m}$, which gives the degree of ionization and also the energy lost in the ionization process. For the typical temperatures that develop in the center of the bubble of $10^6 - 10^7$ K it can easily be seen that multiple ionization is taking place. The equation of state that allows for ionization is

$$\epsilon(T) = \frac{N_a}{\gamma_a - 1}k_b T + \frac{N_m}{\gamma_m - 1}k_b T + \frac{N_a + N_m}{\gamma_e - 1}\overline{m}k_b T + (N_a + N_m)Q(\overline{m}) \ , \quad \text{(C4)}$$

where N_a and N_m are the numbers of atoms and molecules per unit volume, respectively. Here γ_m, γ_a, and γ_e are the heat capacity ratios for molecules, atoms, and electrons, respectively. $Q(\overline{m})$ is the energy required to remove an electron with ionization potential corresponding to $\overline{m}$. The first three terms on the right-hand side of Eq. (C4) are internal energies corresponding to atoms, molecules, and electrons, respectively. The electronic excitation energies were neglected in the above equation. The last term in Eq. (C4) was included in Eq. (9) as mechanical energy loss.

APPENDIX D: THERMAL APPROACH

Inclusion of radiation losses involves the coupling of the radiative transfer equation

$$\frac{1}{c}\frac{\partial I_\nu}{\partial t} + \hat{\Omega} \cdot \nabla I_\nu = \kappa'_\nu(I_{\nu p} - I_\nu) \quad \text{(D1)}$$

with the gas dynamics equations. In Eq. (D1) I_ν is the radiative intensity of the body, $I_{\nu p}$ is the equilibrium Planck distribution given by $I_{\nu p} = 2h/c^2 \ \nu^3(e^{\frac{h\nu}{k_B T}} - 1)^{-1}$, and κ'_ν is the attenuation coefficient. All these quantities depend on the frequency ν. Here c is the speed of light and T is the temperature. Equation (D1) is based on the principle of detailed balance and is written in a form applicable for spherically symmetric problems. The unit vector $\hat{\Omega}$ specifies the direction of photon propagation. In order to simplify the space integration, we assume the radiation propagates in the radial direction. The full treatment of the radiative transfer equation is a complicated problem in itself. Since other quantities entering Eq. (D1) (for example, the attenuation coefficient) are not known precisely, our approximate treatment of Eq. (D1) is satisfactory. More exact treatments of radiative transfer for the conditions common in astrophysics can be found in [26]. It should be noted that Eq. (D1) is not limited to the case where the size of the system is large compared to the wavelength of photon. Equation (D1) is a statement of local conservation of energy for the electromagnetic part of the energy. The left-hand side is essentially Poynting's theorem and the right-hand side includes energy sources and sinks. At thermal equilibrium $I_{\nu p} = I_\nu$ and the sources cancel the sinks. Thus the right-hand side describes phenomenologically how absorption and emission relate to other at low radiation intensities. It is an approximation to use for κ'_ν the photon absorption coefficient. However, in comput-

ing κ'_ν from first principles it is the local electric field $E(t)$ that determines the loss processes and this field exists at all length scales. To the extent that the local field equals the radiation field, κ'_ν can be estimated as being equal to the photon absorption coefficient. Further simplification is found by assuming equilibrium between the radiation and matter. It can easily be seen from Eq. (D1) that the time t_p, required for the equilibrium to be established, is of the order of $1/(c\kappa'_\nu)$.

The value of the attenuation coefficient is sufficiently high to make t_p short compared to the time bubble spends close to the minimum. [For T in the range of 10^5-10^6 K and frequencies near the maximum of the Planck spectrum of 10^{16} Hz, κ'_ν is typically $10^5-10^6\,\mathrm{cm}^{-1}$ (see Table I). Thus t_p is on the order of 10^{-15} s, which is much shorter than the time the bubble spends close to the minimum radius.] This occurs for frequencies at which most of the energy is emitted. This effectively says that Eq. (D1) can be employed without the time derivative term. Solving this simplified equation (D1) and calculating the energy flux $S_\nu(r,t)$ through a spherical surface of radius r from the radiative intensity, the energy flux per unit area is given by $\vec{S}_\nu(\vec{r},t)=\int I_\nu(\vec{r},\hat{\Omega},t)\hat{\Omega}\,d\hat{\Omega}$. Using the condition of thermodynamic equilibrium and spherical symmetry of our problem, the radial flux $S_\nu(r,t)$ was calculated [26]. Finally, we obtain the following result for the energy loss per unit mass during the time Δt in the shell of width Δr:

$$\Lambda(r,t)=\frac{\Delta t}{m(\Delta r)}\int_0^\infty [S_\nu(r,t)-S_\nu(r-\Delta r,t)]d\nu\ , \quad \text{(D2)}$$

where $m(\Delta r)$ is the mass in the shell and r is the distance from the bubble center.

The properties of matter enter Eqs. (D1) and (D2) through the attenuation coefficient κ'_ν. This quantity involves all processes that are responsible for absorption or emission of radiation. The model for the attenuation coefficient is given in the following appendix.

APPENDIX E: CALCULATION OF THE ABSORPTION COEFFICIENT

Electronic transitions that are connected with emission or absorption of light can be divided into three types: free-free transitions (bremsstrahlung emission and absorption), bound-free transitions (photoelectric absorption), and bound-bound (discrete) transitions. From an energy point of view, continuous transitions (free-free or bound-free) are of primary interest. At the temperatures that are of interest to us (5×10^4 K or more) it can be assumed that air molecules are mostly dissociated and atoms are multiply ionized. Thus, in what follows we are going to limit our treatment to these conditions and neglect additional complications (such as molecular transitions). The attenuation coefficient κ_ν, in principle, consists of an absorption part $\kappa_{\nu a}$ and a scattering part $\kappa_{\nu s}$. Scattering (mainly photon scattering from electrons, known as Thomson scattering) is usually important only in a very rarefied gas. The reason for this is that the cross section for scattering is much smaller than the cross section for absorption. Only at low densities and high temperatures does scattering become important. Under these conditions full ionization takes place, so the bound-free transitions are absent and the free-free transitions are small. The latter are proportional to the square of the gas density. The absorption coefficient $\kappa_{\nu a}$ (we are going to drop the subscript a in what follows) should be corrected for induced emission and leads to the following expression for the effective absorption coefficient:

$$\kappa'_\nu=\kappa_\nu(1-e^{-\frac{h\nu}{k_BT}})\ . \quad \text{(E1)}$$

This is what appears in Eqs. (D1) and (D2). The calculation of the absorption coefficient itself is extremely involved and requires a detailed knowledge of the structure of gas. The best one can hope for is to get good approximate results for this quantity. The result, which includes bound-free and free-free transitions in the hydrogenlike approximation for atoms (Kramers-Unsöld formula) used for the conditions of multiple ionization, is [22]

$$\kappa_\nu=\sum_m \kappa_{\nu m}\ , \quad \text{(E2)}$$

$$\kappa_{\nu m}=\frac{aN_m(m+1)^2}{T^2}e^{-x_{1m}}F_m(x)\ , \quad \text{(E3)}$$

where

$$a=\frac{16\pi^2}{3\sqrt{3}}\frac{e^6}{hck_B^2},\quad x=\frac{h\nu}{k_BT},\quad x_{1m}=\frac{I_{m+1}}{k_BT}\ , \quad \text{(E4)}$$

and the frequency dependence of function $F_m(x)$ is given by

$$F_m(x)=\begin{cases} e^x/x^3 & \text{if } x<x_{1m} \\ 2x_{1m}e^{x_{1m}}/x^3 & \text{if } x>x_{1m}\ , \end{cases} \quad \text{(E5)}$$

where N_m is the number of ions per unit volume with charge m and I_m is the ionization potential for removing $m-1$ electrons. The m sum can be omitted by going to the continuum limit, as discussed before. The contributions of bound-free (photoelectric effect) and free-free (bremsstrahlung absorption) transitions to the total absorption coefficient are in the ratio $(e^x-1)/1$. Thus, for the low-energy photons ($x\ll1$), the main contribution comes from free-free transitions, and for the high-energy photons ($x\gg1$), the main contribution comes from bound-free transitions. In our problem, in which there is a wide range of frequencies and temperatures, both kinds of transitions are going to be important in the absorption process.

APPENDIX F: BREMSSTRAHLUNG MODEL

The radiation cross section $d\chi/d\omega$ for the bremsstrahlung can be obtained using the Born approximation (Bethe-Heitler formula; see, for example, [27]). The result for the radiation cross section for

bremsstrahlung radiation emitted during "collision" of an electron and singly ionized ion in the nonrelativistic approximation [27] (without correction for the rest of plasma) is

$$\frac{d\chi}{d\omega} = \frac{16}{3}\frac{e^2}{c}\left(\frac{e^2}{m_e c^2}\right)\left(\frac{c}{v}\right)^2 \times \ln\left[\lambda' \frac{(\sqrt{E}+\sqrt{E-\hbar\omega})^2}{\hbar\omega}\right]\Theta(E-\hbar\omega)\ . \quad \text{(F1)}$$

In the Born approximation the factor λ' is equal to one. In Eq. (F1) E, v, and m_e are the electron energy, velocity, and mass, respectively. The Θ function enters in because the electron energy has to be larger than the energy of the emitted photon. The result for the energy radiated per unit time per unit frequency per unit volume is

$$\frac{dE}{d\omega\ dV\ dt} = \left\langle v\ \frac{d\chi}{d\omega}\right\rangle n_e n_{\rm ion}, \quad \text{(F2)}$$

where n_e and $n_{\rm ion}$ are the concentrations of electrons and ions, respectively, and $\langle v\ d\chi/d\omega\rangle$ represents the thermal average of the product of the electron velocity v and the radiation cross section. It is assumed that the electron gas and ions are at the same temperature (the relaxation time is fairly short, as seen before) and that the velocity of the electrons satisfies the Maxwell distribution (the relaxation time for establishing a Maxwell distribution is short compared to the time scale that is of interest to us). The result for this thermal average is given by

$$\left\langle v\ \frac{d\chi}{d\omega}\right\rangle = \frac{64\pi}{3}\frac{e^2}{c}\left(\frac{e^2}{m_e c^2}\right)\left(\frac{\beta m_e}{2\pi}\right)^{3/2} I(\beta,\omega)\ , \quad \text{(F3)}$$

where $\beta = 1/(k_B T)$ is Boltzmann factor and the integral I is given by

$$I(\beta,\omega) = \int_{\hbar\omega}^{\infty} e^{-\beta E} \ln\left[\frac{\left(\sqrt{E}+\sqrt{E-\hbar\omega}\right)^2}{\hbar\omega}\right] dE\ . \quad \text{(F4)}$$

By partial integration, this integral can be written in the form

$$I(\beta,\omega) = \frac{1}{\beta}\int_1^{\infty} \frac{e^{-\beta\omega\hbar x}}{\sqrt{x(x-1)}}\ dx\ , \quad \text{(F5)}$$

where $x \equiv E/(\hbar\omega)$.

The next step is to include corrections to individual scattering events that lead to radiation because of the presence of the rest of the plasma. These corrections can be included by noting that (in the dipole approximation) the electric dipole $\mu(\omega)$, in a cavity with dielectric constant $\epsilon(\omega)$, emits radiation as it if had an effective dipole moment $\vec{p}(\omega) = 3/[2+\epsilon(\omega)]\,\vec{\mu}(\omega)$. (This result is independent of the location or orientation of the dipole.) Here $\epsilon(\omega)$ is the plasma dielectric constant given by

$$\epsilon(\omega) = 1 - \frac{\omega_p^2}{\omega\ (\omega + \frac{i}{\tau})}\ , \quad \text{(F6)}$$

where ω_p is the plasma frequency and τ is the electron collision time. This collision time is assumed to result from Coulomb scattering of electrons and is given by $1/\tau = n_e v \sigma_C$, where n_e is the electron density, v is the electron velocity, and σ_C is the Coulomb cross section. In this approximation it is assumed that the cavity has well defined walls, i.e., that the electron density falls rapidly over a short distance. Finally, after inclusion of above mentioned correction, one gets the following result for the emitted energy per unit volume per unit time:

$$\frac{dE}{dt\ dV} = \frac{64\pi}{3}\frac{e^2 c}{m_e}\left(\frac{e^2}{m_e c^2}\right)^2\left(\frac{\beta m_e}{2\pi}\right)^{3/2} \times \frac{\omega_p}{\beta} n_e n_{\rm ion} F(\beta\hbar\omega_p, \omega_p\tau)\ , \quad \text{(F7)}$$

where e and m_e are the electron charge and mass, respectively, and $\beta = 1/(k_B T)$. The function F is given by

$$F(\beta\hbar\omega_p, \omega_p\tau) = \frac{1}{\omega_p}\int_0^{\infty} d\omega \times \int_1^{\infty} dx \frac{e^{-\beta\hbar\omega x}}{\sqrt{x(x-1)}}\left|\frac{3}{2+\epsilon(\omega)}\right|^2\ . \quad \text{(F8)}$$

The function F was calculated numerically and, finally, the energy loss given by Eq. (F7) was included in the loss term on the right-hand side of Eq. (5). The calculations were carried through by introducing a cutoff in order to define the size of the plasma region around the bubble center where bremsstrahlung takes place. This cutoff was defined in terms of the critical degree of ionization m_c. The plasma region was defined as one where the degree of ionization m is larger than m_c. The results for the energy loss are not very sensitive to the choice of m_c, which was taken to be 1.0 in the actual calculations.

[1] L.A. Chambers, J. Chem. Phys. **5**, 290 (1937).
[2] B.P. Barber and S.J. Putterman, Nature **352**, 318 (1991).
[3] R. Hiller, S.J. Putterman, and B.P. Barber, Phys. Rev. Lett. **69**, 1182 (1992).
[4] B.P. Barber and S.J. Putterman, Phys. Rev. Lett. **69**, 3839 (1992).
[5] C.C. Wu and P.H. Roberts, Phys. Rev. Lett. **70**, 3424 (1992).
[6] C.C. Wu and P.H. Roberts, Adv. Phys. **33**, 595 (1994).
[7] W.C. Moss, D.B. Clark, J.W. White, and D.A. Young, Phys. Fluids **6**, 2979 (1994).
[8] B.P. Barber, C.C. Wu, R. Lofstedt, P.H. Roberts, and S.J. Putterman, Phys. Rev. Lett. **72**, 1380 (1994).
[9] A.J. Walton and G.T. Reynolds, Adv. in Phys. **33**, 595

(1984).
[10] Lord Rayleigh, Philos. Mag. **34**, 94 (1917).
[11] S.K. Godunov, Math. Sbornik **47**, 271 (1959).
[12] M. Holt, *Numerical Methods in Fluid Dynamics* (Springer-Verlag, New York, 1977).
[13] M.S. Plesset and D.Y. Hsieh, J. Appl. Phys. **23**, 95 (1951).
[14] M.S. Plesset and D.Y. Hsieh, Phys. Fluids **3**, 882 (1960).
[15] E.A. Neppiras, Phys. Rep. **61**, 159 (1984).
[16] H.G. Flynn, J. Acoust. Soc. Am. **57**, 1379 (1975).
[17] L.A. Crum, J. Acoust. Soc. Am. **73**, 116 (1983).
[18] L.A. Crum, J. Acoust. Soc. Am. **73**, 121 (1983).
[19] A. Prospereti, Ultrasonics **22**, 69 (1984).
[20] A. Prospereti, Ultrasonics **22** , 115 (1984).
[21] A. Prospereti and A. Lezi, J. Fluid Mech. **168**, 457 (1986).
[22] Ya. B. Zeldovich, *Physics of Shock Waves and High Temperature Hydrodynamic Phenomena* (Academic, New York, 1966).
[23] G. Guderley, Luftfahrtforschung **19**, 302 (1942).
[24] R. Hiller, K. Weninger, S.J. Putterman, and B.P. Barber, Science **266**, 248 (1994).
[25] *Handbook for Chemistry and Physics*, 72nd ed. (MIT Press, Cambridge, MA, 1992).
[26] D. Mihalas, *Stellar Atmospheres* (Freeman, San Francisco, 1978).
[27] J.D. Jackson, *Classical Electrodynamics* (Wiley, New York, 1975).